10B.4 THE NOAA COASTAL ATMOSPHERIC RIVER OBSERVATORY

Allen B. White*, F. Martin Ralph, Paul J. Neiman, Daniel J. Gottas, and Seth I. Gutman
NOAA Earth System Research Laboratory, Boulder, Colorado

1. INTRODUCTION

Atmospheric rivers (ARs) have emerged as a phenomenon that is key to both the global water cycle (e.g., Zhu and Newell, 1998) and to extreme precipitation events and flooding in large geographical areas (e.g., Ralph et al. 2006; Leung et al. 2009). Their importance arises from the role they play in focusing horizontal water vapor transport in relatively narrow ribbons (i.e., "rivers") that are roughly 400 km wide on average. Upon making landfall, the mesoscale conditions within ARs create heavy orographic precipitation (Ralph et al. 2005; Neiman et al. 2002, 2008). Figure 1 shows a characteristic SSM/I satellite image of an AR striking the California coast. The heavy rain associated with this AR led to high stream flow in watersheds along a large stretch of coastal northern California.

While the vertically integrated water vapor measurements from satellites have provided a key tool for detecting AR conditions offshore (Ralph et al. 2004), the data suffer from several key limitations, including the absence of wind measurements, the inability to make measurements over land, and the relative infrequency of the polar-orbiter overpasses. Based on these gaps, and on the demonstrated ability of wind profilers to monitor horizontal winds aloft with the necessary vertical and temporal resolutions (White et al. 2007), as well as the ability of GPS-met receivers to monitor IWV from the ground (Bevis et al. 1992), a combination of the two have been fielded to monitor AR conditions at the coast. Because ARs play such a crucial role in generating orographic precipitation, the coastal water vapor transport monitoring capabilities have been supplemented with research-quality precipitation measurements in the mountains downwind of the coastal site.

Given the importance of ARs for both short-term weather prediction (i.e., to anticipate extreme precipitation) as well as for understanding how changes in climate could impact the frequency, intensity, and other characteristics of extreme precipitation and flooding on the U.S. West Coast, it was recognized that continuous measurements were needed in real time and that long-term monitoring was necessary. Because earlier research studies deployed key elements of this array, some of the key data already go back more than ten years at two key West Coast sites. Based on this experience and on the long-term requirements, the concept has evolved to operate these sites as "observatories."

The purpose of this paper is to document the key observational requirements and methodologies developed to monitor AR conditions along the U.S. West Coast. A historical perspective is provided that describes key scientific and technical advances that led to the creation of an AR observatory (ARO). In addition to documenting what has been developed to date, this paper also provides a foundation for potential additional ARO deployments that are either already underway or are under consideration.

2. EARLY CALJET FINDINGS

This section summarizes some of the early research results from the California Land-falling Jets Experiment (CALJET; January–March 1998) that form the building blocks for the more recent results that will be presented later in this paper. For more complete descriptions of these earlier results, consult the referenced literature.

During CALJET, scientists from the Earth System Research Laboratory (ESRL) and their colleagues began studying the winter storms that lead to dangerous flooding and debris flows along the U.S. West Coast. One of the geographical regions of focus during CALJET was the Russian River watershed north of San Francisco. This watershed was chosen because of its relatively frequent recurrence of flooding and the operational forecast challenges that result.

Realizing that the coastal orography likely would play a substantial role in enhancing precipitation, ESRL scientists designed a ground-based observing strategy for CALJET to

---

* *Corresponding author address:*
Dr. Allen B. White, NOAA/ESRL, R/PSD2,
325 Broadway, Boulder, Colorado, 80305
e-mail: allen.b.white@noaa.gov

complement offshore research flights conducted with the NOAA P-3 Orion aircraft. The instruments deployed in the vicinity of the Russian River consisted of a 915-MHz Doppler wind profiler (Carter et al. 1995) along with a collocated 10-m meteorological tower deployed at the coast and a vertically-pointing, S-band (2875-MHz) precipitation profiling radar (S-PROF; White et al., 2000) along with a 10-m meteorological tower located 34.5 km to the northwest in the coastal mountains (see Fig. 2). The 10-m tower deployed at each location recorded 2-min. average measurements of pressure, temperature, and relative humidity at 2 m above ground level (AGL); wind speed and direction at 10 m AGL; incoming solar and net radiation; and surface rainfall.
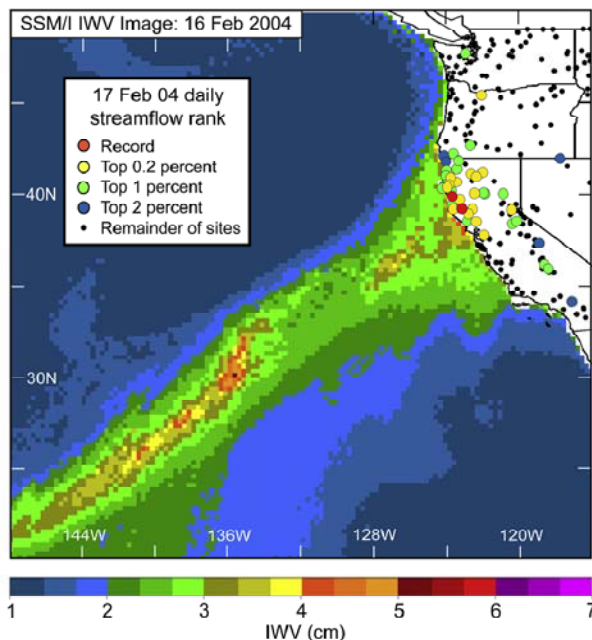

Figure 1. *Composite SSM/I satellite image of IWV (cm; color bar at bottom) constructed from polar-orbiting swaths between ~1400 and 1830 UTC 16 February 2004 and ranking of daily streamflows (percent; see inset key) on 17 February 2004 for those gauges that have recorded data for ≥30 years. The streamflow data are based on local time (add 8 h to convert to UTC). From Ralph et al. (2006).*

2.1 Low-level Jets Impact Precipitation

An observational study by Neiman et al. (2002) statistically linked hourly rainfall rates observed in California's quasi-linear coastal mountains to the hourly averaged upslope component of the flow measured by coastal wind profilers immediately upstream. In addition to the observing couplet described earlier and shown in the inset of Fig. 2, two additional observing couplets were deployed further south along the California Coast during CALJET (Fig. 2). The two southern couplets used wind profilers and 10-m meteorological towers at the coast, whereas the coastal mountain sites consisted only of rain gauges that were part of the operational rain-gauge network operated by California.
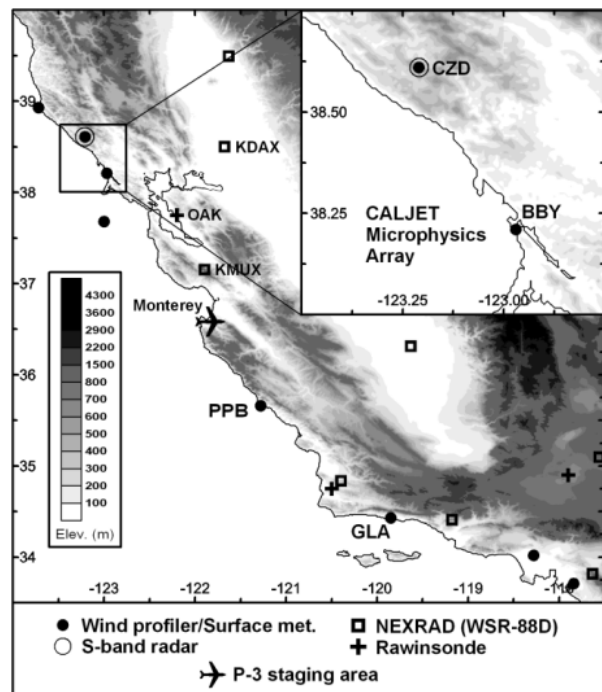

Figure 2. *Basemap of California showing the locations of key observing sites employed during CALJET. The map inset shows the northern observing couplet consisting of sites at Bodega Bay (BBY) and Cazadero (CZD). Two other observing couplets referred to in Section 2.1 were organized around the wind profilers located at Point Piedras Blancas (PPB) and Goleta (GLA). After White et al. (2003).*

Using these three locations with differing coastal terrain characteristics, Neiman et al. (2002) found that the layer of upslope flow that optimally modulates orographic rainfall was near mountaintop, that is, about 1 km above mean sea level (MSL) for California's coastal ranges. The correlation coefficient in this layer was largest when the upslope flow was compared to rainfall rates from the coastal mountain sites rather than

from the coastal sites, thus further highlighting the physical connection between upslope flow and orographic rainfall in the coastal mountains. The height of maximum correlation also corresponded to the mean altitude of a baroclinically-forced, landfalling low-level jet (LLJ) that was observed by the coastal wind profilers and by the NOAA P-3 aircraft offshore. For example, Fig. 3 shows the winter season correlation coefficient profile for upslope flow versus rain rate for the northern couplet (Fig. 2). Shown for comparison is a composite wind profile measured offshore from the NOAA-P3 during ten different events.
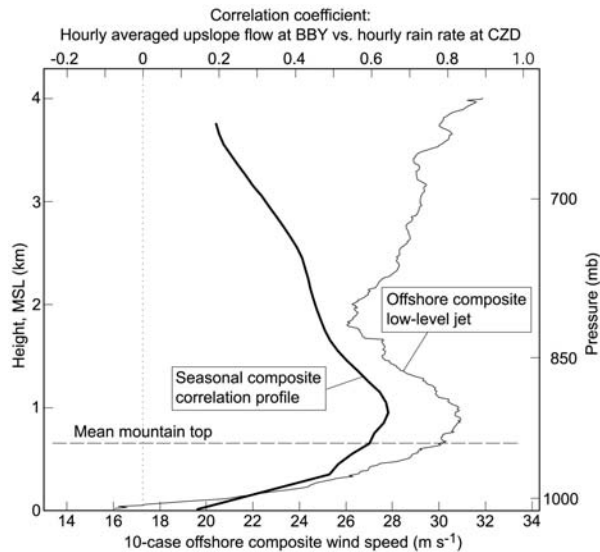

Figure 3. Seasonal (Jan.–Mar. 1998) *vertical profile of the linear correlation coefficient between the hourly averaged profile of upslope flow measured at BBY versus the hourly rainfall rate measured at CZD (bold curve; use top axis). Composite vertical profile of wind speed based on NOAA P-3 flight-level and dropsonde measurements taken over the eastern Pacific Ocean during ten CALJET storms that contained an LLJ (thin curve; use bottom axis). After Neiman et al. (2002).*

On average, the presence of shallow, terrain-blocked flow modulated the seasonal correlation coefficient profile below mountaintop, such that the low-level flow at the coast was poorly correlated with rain rates observed in the coastal mountains (Fig. 3). However, individual cases without significant blocking retained relatively large correlation coefficient values below mountaintop (not shown).

These results by Neiman et al. (2002) highlight the need to measure the winds aloft, especially to resolve the upslope component of the LLJ. The 915-MHz wind profilers deployed during CALJET and subsequent West Coast research field programs are ideally suited for this purpose, but they don't provide much lead time for operational weather forecasters to anticipate and forecast the heavy orographic precipitation, flooding, and debris flows that may ensue. Unfortunately, there is not a routine method in existence to measure LLJs offshore, and a dedicated winter storms reconnaissance program using aircraft, akin to the annual hurricane effort in the Eastern U.S., likely would be required to provide that capability.

2.2 *Snow Levels Impact Streamflow*[1]

White et al. (2002) used the National Weather Service River Forecast System (NWSRFS) configured by the NWS California-Nevada River Forecast Center (CNRFC) to study the sensitivity of runoff to the snow level, defined here as the lowest altitude in the atmosphere where snow or ice completely changes to rain. In reality, melting occurs over a layer of finite thickness, the top of which corresponds to the melting level, or 32 °F isotherm. Because the operational weather forecast models used to drive the NWSRFS provide forecasts of the melting level and the natural variability associated with the vertical displacement between the melting level and the snow level, White et al. (2002) used the melting level in their sensitivity studies. Figure 4 shows the locations of the four Northern California watersheds used in this study. Other characteristics of these watersheds, including basin area, response time, and flood stage are provided in White et al. (2002).

A modest 24-h quantitative precipitation forecast, in 6-h increments of 0.5, 1.5, 1.5, and 0.5 in., was used to drive the runoff model. Beforehand, each basin was brought to a midwinter soil moisture condition by adjusting parameters in the model. Successive model runs, each using a different melting level ranging from low to high elevations within each basin, were made using the same specified precipitation

---

[1] To be consistent with the units used in the original publication and by the National Weather Service, English units are used throughout section 2.2.

forecast. The peak streamflow for each run was recorded and plotted as a function of melting level in Fig. 5. The increase in runoff with increasing altitude of the melting level is quite evident. In some watersheds this increase is abrupt over a small range of melting levels. For example, in three of the four watersheds examined, the runoff triples when the melting level is raised by 2000 ft.
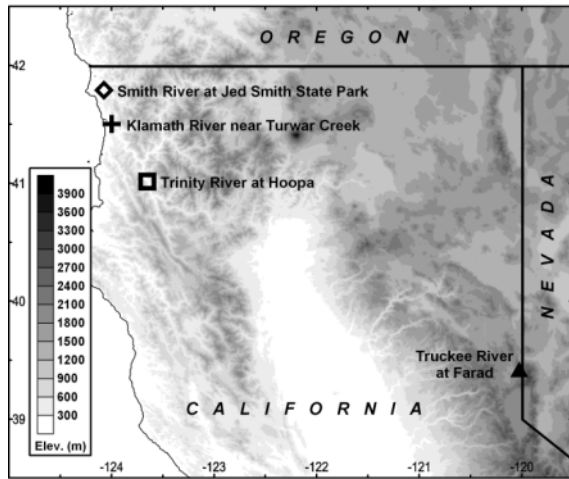

Figure 4. *Basemap of Northern California showing the locations where the impact of the melting level on streamflow was evaluated.*

Based on the need to monitor the melting level to verify weather model forecasts used in hydrometeorologic prediction, White et al. (2002) developed an algorithm[2] to automatically detect the radar brightband height during precipitation. The *bright band* (BB) is a layer of enhanced radar reflectivity resulting from the difference in the dielectric factor for ice and water and the aggregation of ice particles as they descend and melt. The *brightband height* (BBH) is the altitude of maximum radar reflectivity in the BB. The BBH exists below the melting level in the melting layer and is a better estimate of the snow level than the melting level because of the distance required for frozen precipitation particles to melt as they fall through the melting layer.

The algorithm works well with the Doppler wind profilers and S-PROFs that ESRL has deployed for research projects at many sites throughout the U.S. During winter, BBH data are available publicly on a real-time data Web site (http://www.etl.noaa.gov/et7/data/). An example of

---

[2] U.S. Patent # 6,615,140

the online display is shown in Fig. 6. In 2008, ESRL began developing a portable, frequency-modulated, continuous wave (FMCW) S-band radar for the California Department of Water Resources. This radar uses extremely little power (a few Watts) and is, therefore, an order of magnitude less expensive to produce than the pulse-transmitted S-PROF and 915-MHz wind profilers.
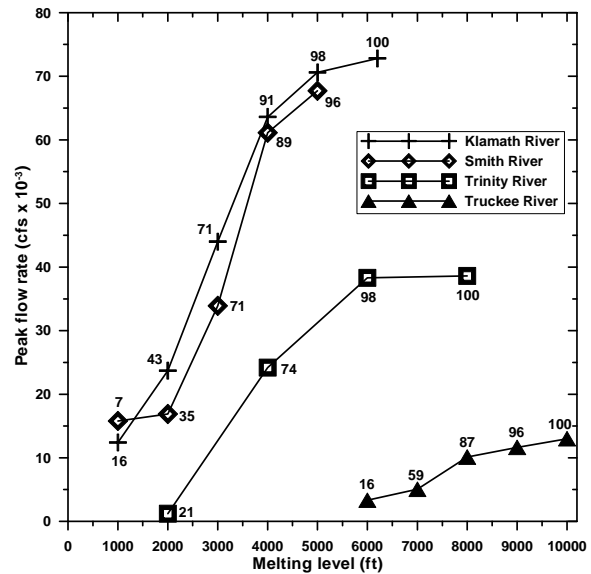

Figure 5. *River forecast model simulations of the sensitivity of runoff to changes in melting level for four river basins in California (basin symbols defined in Fig. 4). The posted numbers give the approximate percentage of basin area below the altitude corresponding to the melting level. These percentages were determined by linearly interpolating the area elevation curves generated for each basin. From White et al. (2002).*

2.3 *Nonbrightband Rainfall Process*

White et al. (2003) used radar reflectivity and Doppler vertical velocity measurements from the S-PROF deployed at Cazadero, California, to document a shallow, orographic, quasi-steady, nonbrightband (NBB) rain process and compared this structure to what is found in the much more well-documented brightband (BB) rain (e.g., Battan 1959; Anagnostou and Kummerow 1997). Figure 7a shows the distinctively different patterns of radar reflectivity and Doppler vertical velocity associated with each rainfall process. NBB rain consistently occurred with weaker radar reflectivity and smaller Doppler vertical velocity than BB rain

for rainfall events that produced nearly equivalent rain rates, implying that NBB rain consists of smaller drops. This hypothesis was confirmed later by Martner et al. (2008), who used drop-size distributions measured with an impact disdrometer to illustrate the remarkably different microphysical properties of BB and NBB rain. Figure 7b illustrates the difficulty in observing the shallow NBB rain process using the operational WSR-88D radars in California.
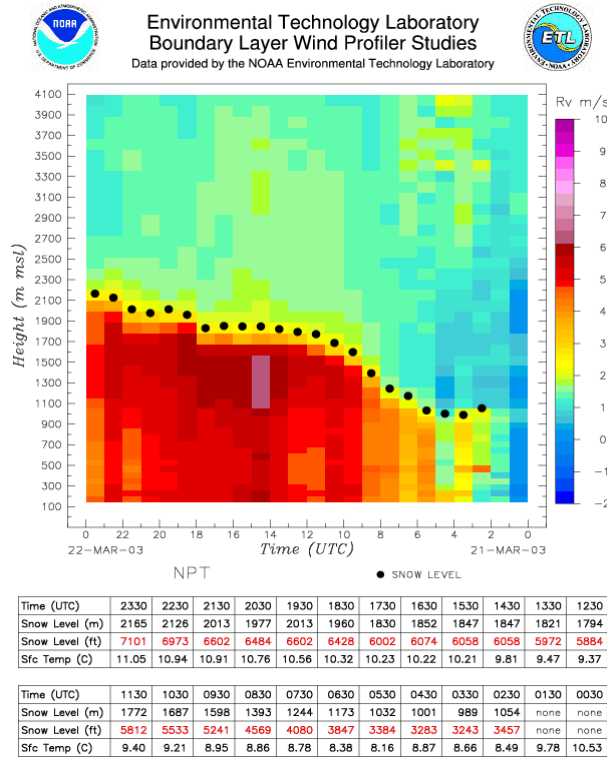

Figure 6. *Example of the snow-level product displayed on the Web (www.etl.noaa.gov/et7/data) during a precipitation event. The background colors indicate the Doppler vertical velocity (m s⁻¹; positive downward). The snow levels are indicated by the black dots and listed in the table below along with the 2-m air temperature. Time proceeds from right to left on the bottom axis. The data were collected on March 21, 2003, with a 915-MHz wind profiler and collocated meteorological tower deployed at Newport, Oregon.*

The snow levels are indicated as follows:

Time (UTC)	2330	2230	2130	2030	1930	1830	1730	1630	1530	1430	1330	1230
Snow Level (m)	2165	2126	2013	1977	2013	1960	1830	1852	1847	1847	1821	1794
Snow Level (ft)	7101	6973	6602	6484	6602	6428	6002	6074	6058	6058	5972	5884
Sfc Temp (C)	11.05	10.94	10.91	10.76	10.56	10.32	10.23	10.22	10.21	9.81	9.47	9.37

Time (UTC)	1130	1030	0930	0830	0730	0630	0530	0430	0330	0230	0130	0030
Snow Level (m)	1772	1687	1598	1393	1244	1173	1032	1001	989	1054	none	none
Snow Level (ft)	5812	5533	5241	4569	4080	3847	3384	3283	3243	3457	none	none
Sfc Temp (C)	9.40	9.21	8.95	8.86	8.78	8.38	8.16	8.87	8.66	8.49	9.78	10.53

3. ATMOSPHERIC RIVERS

Atmospheric rivers (ARs) are narrow regions of enhanced water vapor transport in the warm sector of extratropical cyclones. On any given day, ARs account for over 90% of the global meridional water vapor transport, and yet they take up less than 10% of the Earth's circumference (Zhu and Newell, 1998). A recent study by Ralph et al. (2006) showed that all eight floods occurring on the Russian River between 1997 and 2006 were the result of winter storms containing atmospheric river conditions. ARs are clearly visible from satellite data over the oceans (e.g., Fig. 8). However, satellite methods only measure the integrated water vapor content, i.e., not the winds that transport the water vapor. In addition, as ARs strike land, the satellite water vapor retrieval methods do not work.
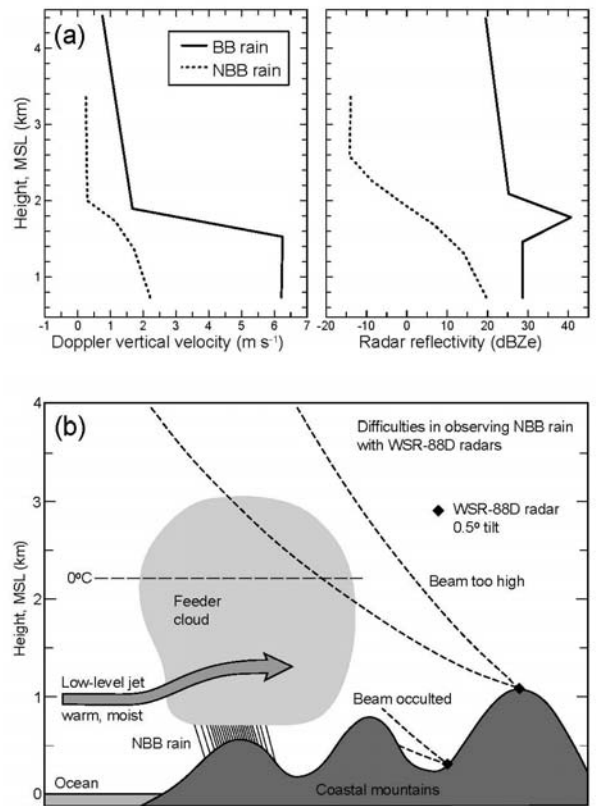

Figure 7. *(a) Composite winter-season profiles of Doppler vertical velocity (m s⁻¹; positive downward) and equivalent radar reflectivity factor (dBZe) measured by a vertically pointing, S-band precipitation profiler (S-PROF) during brightband (BB) rain (solid) and nonbrightband (NBB) rain (dashed). The average rain rate for each rain type is approximately the same (3.95 mm h⁻¹). (b) Conceptual representation of shallow NBB rain in California's coastal mountains, and the inability of the operational WSR-88D radars to observe it adequately. NBB rain is portrayed falling from a shallow feeder cloud forced by warm and moist onshore flow associated with a land-falling low-level jet (bold arrow). From White et al. (2003).*
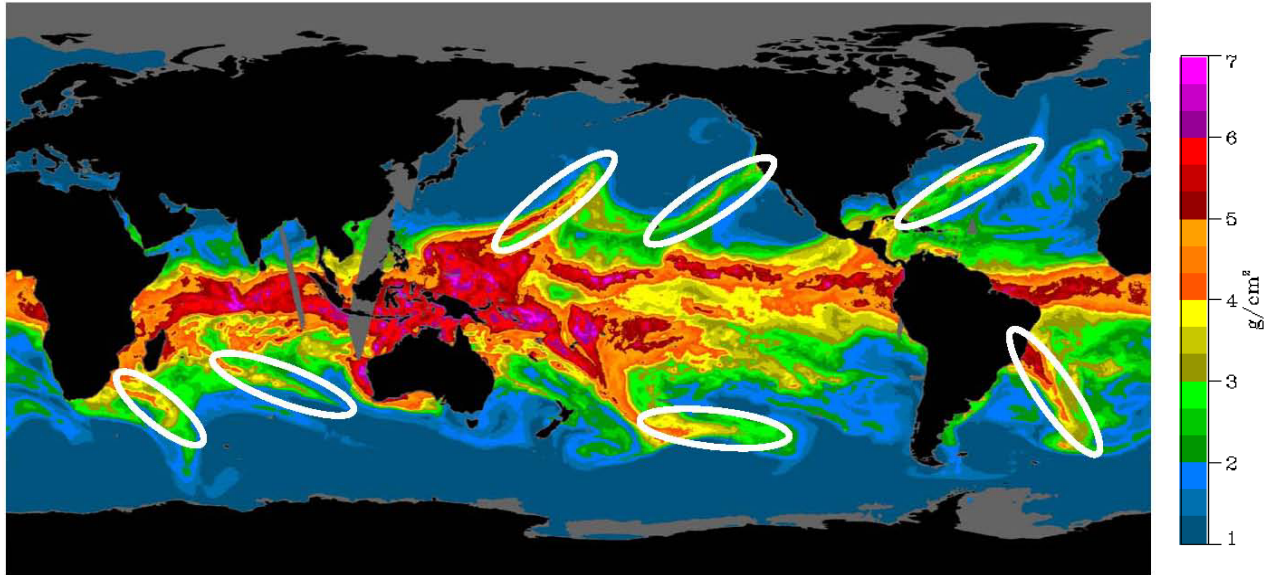
5

Figure 8. *Daily (February 16, 2004) composite satellite image of integrated water vapor (g cm^{-3}) measured by the Special Sensor Microwave Imager (SSM/I) flown aboard several of the Defense Meteorological Satellite Program (DMSP) polar orbiting satellites. Several atmospheric rivers are evident (regions enclosed by white ovals), including one that is making landfall on the U.S. West Coast. This image is courtesy of Gary Wick.*

3.1 *Atmospheric River Thresholds*

Ralph et al. (2004) used Special Sensor Microwave Imager (SSM/I) satellite observations to establish detection thresholds for ARs. Among these were that the core of the moisture plume had to have integrated water vapor (IWV) >2 cm (i.e., the depth of the condensed water in a vertical column of the atmosphere above the receiver). Because ARs are the consequence of moisture confluence and convergence along the polar cold front of an approaching cyclone, ARs coincide with the baroclinic low-level jets described in Section 2.1.

Neiman et al. (2009) monitored the low-level jet and water vapor conditions at the coast using a Doppler wind profiler collocated with a Global Positioning System (GPS) receiver that provides measurements of IWV via the satellite occultation technique (Bevis et al. 1992). They related these measurements to hourly rainfall measurements collected in the coastal mountains. Four winters of data were analyzed when both sets of observations were available. The results are summarized in Fig. 9. The heaviest rainfall rates (≥10 mm hr^{-1}) at the coastal mountain site occurred exclusively when the IWV was ≥2 cm and the upslope component of the wind was ≥12.5 m s^{-1} at the coastal site. Based on these results, Neiman et al. (2009) added the criterion that an

upslope wind >12.5 m s^{-1}, in addition to the 2-cm integrated water vapor criterion, constituted atmospheric river conditions. It is uncertain whether these thresholds are appropriate for other coastal and/or inland regions.

3.2 *Atmospheric Rivers are Warm and Wet*

Not all winter storms impacting the Western U.S. contain ARs based on the AR thresholds described above. However, storms with ARs imbedded within them consistently produce more precipitation than storms without ARs. Neiman et al. (2008) compared the average of all precipitation days in the Sierra Nevada range (observed by rain gauges and snow pillows) to those days associated with landfalling ARs for Water Years 1998–2005. Their analysis (not shown) indicates that AR storms produced 2.0 times the average precipitation and 1.8 times the average snowfall at stations above 1.5 km MSL.

ARs with larger water vapor contents produce heavier precipitation than weaker ARs, but these stronger ARs also are associated with warmer air masses that produce higher snow levels. As described in Section 2.2, this exacerbates the flood risk by exposing a greater portion of a watershed to runoff. Using the same hourly coastal GPS IWV data and coastal mountain rain gage data that were used to produce Fig. 9 along

with snow levels measured with the S-PROF at the coastal mountain site, Neiman et al. (2009) produced Fig. 10, which shows strong correlation ($r=0.9$) between the IWV in ARs and the corresponding snow level in AR- induced precipitation.
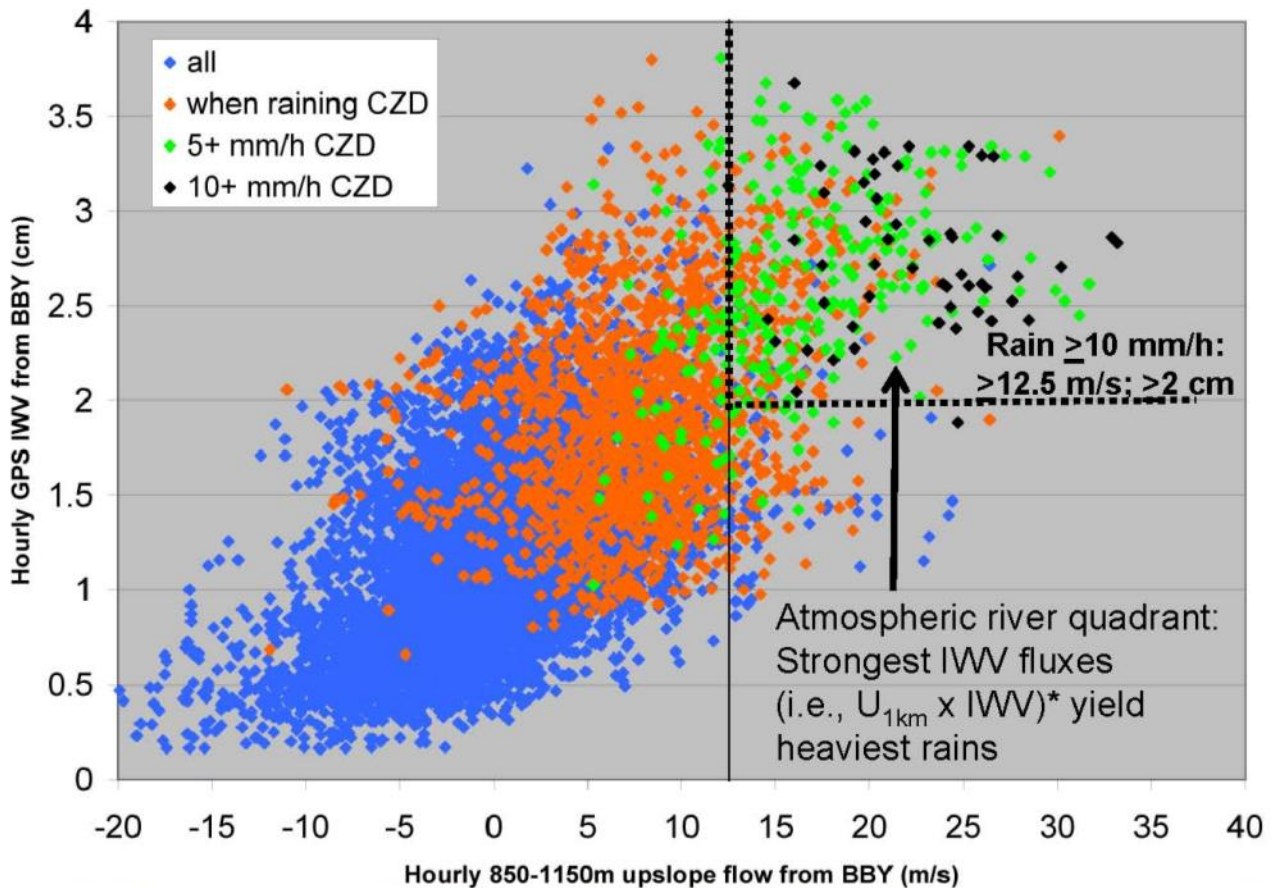

Figure 9. *Hourly integrated water vapor (IWV) as a function of hourly upslope wind speed, both measured at Bodega Bay, California (coastal site), and stratified by whether it is raining at Cazadero, California, (coastal mountain site) with rainfall intensity identified in the upper left. The heaviest rainfall intensities occur when the AR conditions are met. After Neiman et al. (2009).*

4. THE NOAA COASTAL ATMOSPHERIC RIVER OBSERVATORY

The research results presented so far have underscored the importance of detecting ARs and monitoring their impacts over land. To this end, ESRL scientists have developed the concept of an *Atmospheric River Observatory (ARO).* The ARO is composed of a synergistic combination of instruments, shown collectively in Fig. 11, that have been used to develop these results. Table 1 lists the measurements associated with each of the instruments in the ARO. The ARO prototyped in the Russian River area has since been deployed at other regions along the California coast and inland. In some cases, the S-PROF could not conveniently be located in the coastal mountains, so it has been collocated with the wind profiler. Still, in order to measure the orographic precipitation enhancement associated with ARs, it is necessary to have precipitation measurements in the upwind mountain region.

4.1 *The Coastal Atmospheric River Monitoring and Early Warning System*

To provide a method of combining many of the above research results into a single tool, Neiman et al (2009) developed the coastal atmospheric river monitoring and early warning system (CARMEWS). Initially, CARMEWS was an observational display that was updated hourly on

the Web. In February 2009, the tool was modified to include numerical model forecast output at the request of the National Weather Service Forecast Office in Monterey, California. The model used in the tool is a special, rapidly updated version of the Weather Research and Forecasting (WRF) model run at ESRL for NOAA's Hydrometeorology Testbed and similar to the model described in Jankov et al. (2007). There are three panels in the tool's display. Each of these is described in Figs. 12-14. Figure 15 shows all of the information together, as it was displayed publicly on the Web beginning in February 2009.

Figure 10. *Correlation between integrated water vapor (IWV) measured at the Bodega Bay (BBY) coastal site and snow levels measured at the Cazadero (CZD) coastal mountain site over four winter seasons. The correlation coefficient, r, is displayed in the lower right. From Neiman et al. (2009).*

The top panel of the CARMEWS Web display (Fig. 12) contains the observed and forecasted wind profiles and snow levels. As before, the wind profiler derived snow level is the altitude of maximum radar reflectivity in the bright band. For the model, this altitude is represented by the 0 $^{\circ}$C isotherm. White et al. (2009) compared the radar-derived brightband snow levels with temperature profiles measured by rawinsondes launched from the radar sites. They found that the snow level existed, on average, at a temperature of 1.1 $^{\circ}$C.

The middle panel of the CARMEWS Web display (Fig. 14) compares the forecasted and

observed upslope component of the wind and IWV at the coast. The upslope component of the wind is a vertical average (to diminish impact of meteorological noise) calculated in the controlling layer between 850 and 1150 m directed normal to the mean axis of the terrain (Neiman et al. 2002). In this panel, the upslope wind speed in the controlling layer and the IWV can be compared to the individual AR thresholds for these quantities established in Fig. 8 (Neiman et al. 2009).

The bottom panel of the CARMEWS Web display (Fig. 15) compares the forecasted and observed bulk integrated water vapor flux, which is simply the product of the upslope wind speed and the integrated water vapor. This panel also shows the forecasted and observed rainfall at both the coastal and coastal mountain sites. In this case, despite the good agreement between the observations and numerical model for the upslope winds and water vapor, the model substantially underestimated the orographically enhanced rainfall at the coastal mountain site. Figure 14 shows the format of the tool, as it was displayed publicly on the Web beginning in February 2009.

4.2 *Case Study*

During early January 2008, a strong winter storm impacted the U.S. West Coast. In the coastal mountains of California, rainfall exceeding 300 mm in 24 h occurred. The CARMEWS was operated at three sites along the California Coast but prior to the addition of the numerical model information. The coastal wind profilers were located from north to south at BBY, PPB, and GLA (Fig. 3). The corresponding coastal mountain rain gages from north to south were at Cazadero (CZD), Three Peaks (TPK) and San Marcos Pass (SMC). The latter two gauge sites are part of California's automated rain gauge network. For application in the CARMEWS, real-time data from these gauges was provided by the NWS Weather Forecast Office in Monterey, California. Figure 16 shows the bottom panel of the CARMEWS display for the three observing couplets. During AR conditions at each couplet, the enhanced water vapor flux was well correlated with the increased coastal mountain precipitation. In addition, the time of maximum water vapor flux corresponded to the southward propagation of the AR. In this case the AR propagated at an average rate of 12 m s^{-1}. Thus, a network of coastal AROs perhaps would allow weather forecasters to issue more timely forecasts of hazardous winter weather.
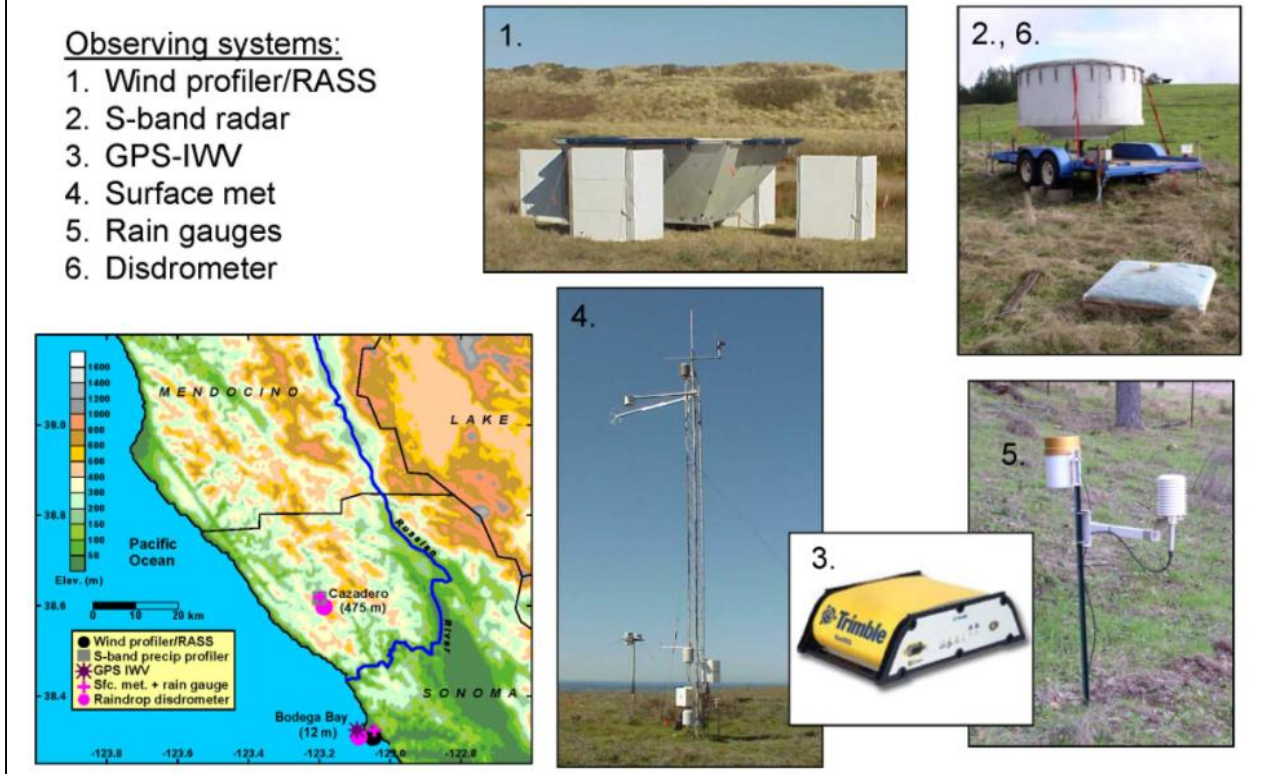
Figure 11. *Instruments used in the ARO and map showing the locations of the ARO deployed near the Russian River in Northern California.*

Table 1. ARO *instrumentation and measurements.*

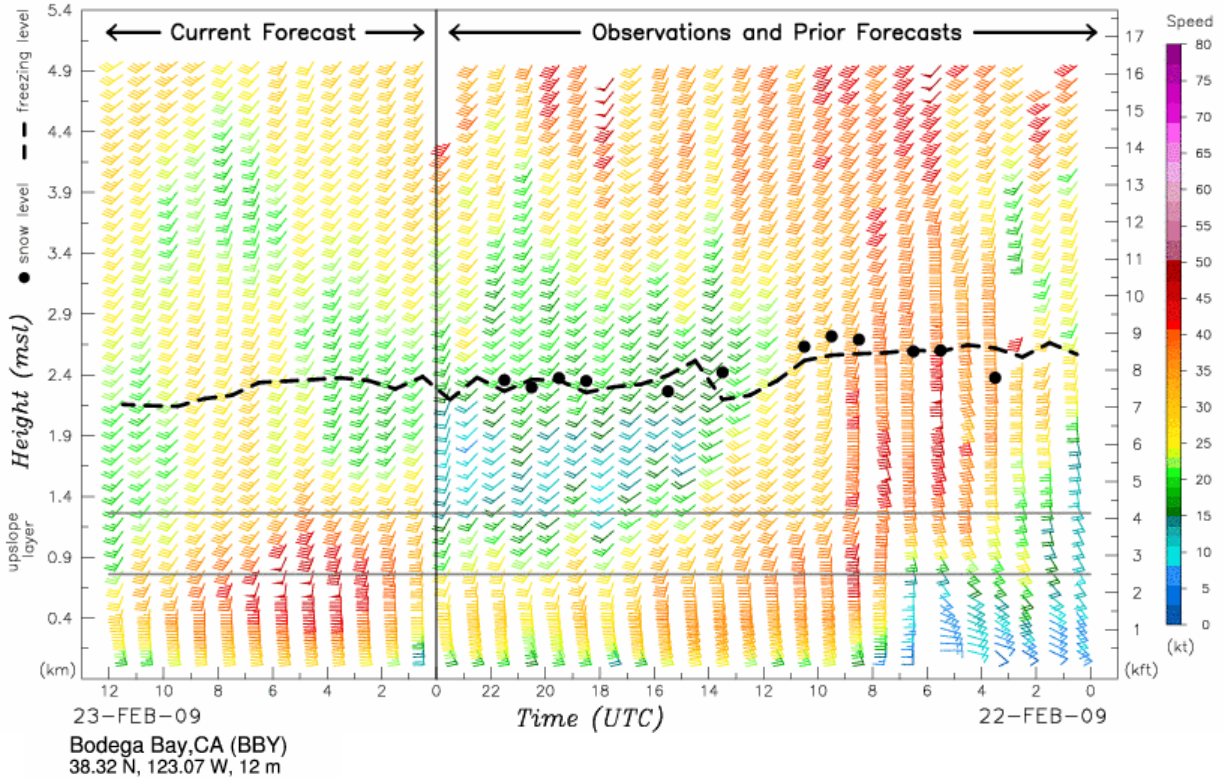| Instrument	Measurements	Vertical Resolution	Temporal Resolution	Altitude Coverage
915-MHz Wind Profiler/RASS	Wind and Virtual temperature (Tv) profiles, Snow level, Boundary-layer depth	60 m, 100 m	Hourly or higher	0.15–2+ km in clear air, 0.15–4+ km in storms (winds); 0.15–1+ km (Tv)
S-band Radar (S-PROF)	Reflectivity and Doppler vertical velocity profiles, Snow level	60 m	30-s	0.13–8+ km in storms
GPS Receiver	Integrated water vapor	N/A	Hourly or higher	N/A
Surface Meteorology (includes rain gauge)	Pressure, Temperature, Relative humidity, Wind speed and direction, Solar and net IR irradiance, rainfall	N/A	2-min.	Surface
Disdrometer	Drop-size distributions	N/A	2-min.	Surface

Figure 12. *Top panel of the coastal atmospheric river monitoring and early warning system Web display. Time proceeds from right to left along the horizontal axis. The vertical line in the left side of the figure denotes the current time. The wind profiles (colored wind barbs; full barb = 5 kt, flag = 50 kt, wind direction indicated by flag pole orientation, color key for speed also shown on the right) and snow levels (black dots) observed over the last 24 h are displayed on the right portion along with the model forecasted melting level (dashed curve). The model forecasted winds and melting level are shown on the left for the latest initialized model run. A new 12-h model run is initialized each hour. In this case the model was last initialized at 0000 UTC on 23 February 2009. The thin horizontal lines denote the controlling layer over which the upslope component of the wind is calculated based on the results of Neiman et al. (2002).*

5.   SUMMARY

A summary of results from more than a decade of winter storm research conducted in California by NOAA's Earth System Research Laboratory (ESRL) and partners since 1998 was given. This research led to the development of an atmospheric river observatory (ARO), a collection of instruments designed to detect and monitor the atmospheric forcing that leads to heavy precipitation along California's coastal and inland mountain ranges. The ARO measures the upslope winds in the controlling layer of the baroclinically-forced low-level jet, which often bear little resemblance to the winds at the surface, highlighting the need to measure the winds aloft. The ARO also measures the vertically integrated water vapor, which is enhanced in atmospheric rivers. Thresholds for each of these quantities

were established to help detect and monitor landfalling atmospheric rivers.

At the request of operational weather forecasters in California, scientists at ESRL used the observations collected by the ARO along with numerical model output to develop a coastal atmospheric river monitoring and early warning system (CARMEWS). The hourly updated Web display from CARMEWS allows weather forecasters and the public to monitor winter storms with imbedded atmospheric rivers and the orographically enhanced precipitation that often results. The addition of numerical model output provides a means for forecasters to evaluate model performance and to calibrate short-term precipitation forecasts on the fly. A goal of future research will be to deploy AROs along the base of the California Sierra Nevada in order to determine how atmospheric rivers change as a result of

10

traversing the Coast Range. This research is part of the motivation for a California Energy Commission research project called CalWater, which plans to have a major field experiment during the winter of 2009–2010.
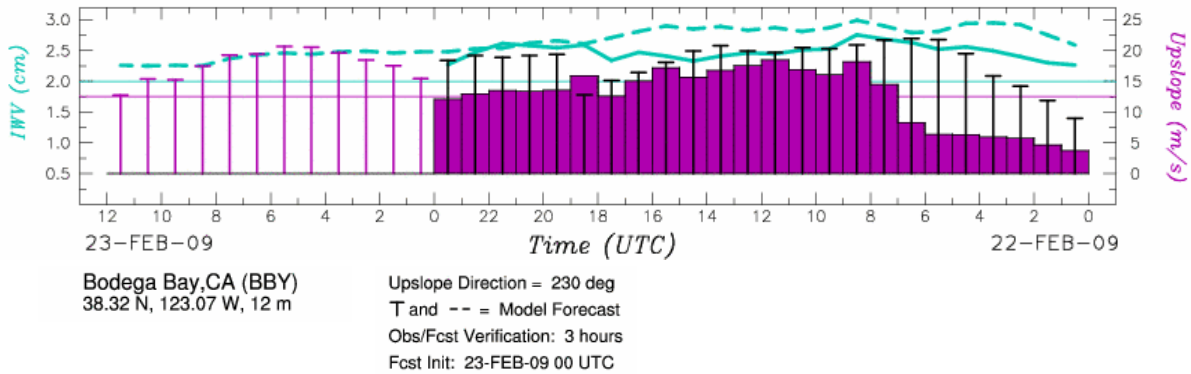

Figure 13. *Middle panel of the coastal atmospheric river monitoring and early warning system Web display. Time proceeds from right to left along the horizontal axis. The hourly upslope flow (from the terrain orthogonal direction of 230 deg) measured by the wind profiler in the controlling layer is represented by the solid vertical bars. The model forecasted upslope flow is represented by the T posts. The forecasted and observed integrated water vapor (IWV) are indicated by the dashed and solid cyan curves, respectively. The thin horizontal lines represent the atmospheric river thresholds for upslope flow and IWV established by Neiman et al. (2009). For the model forecast verification period (i.e., 0000 UTC 22 February 2009 – 0000 UTC 23 February 2009) each hourly observation is compared to a 3-h forecast from the numerical model.*
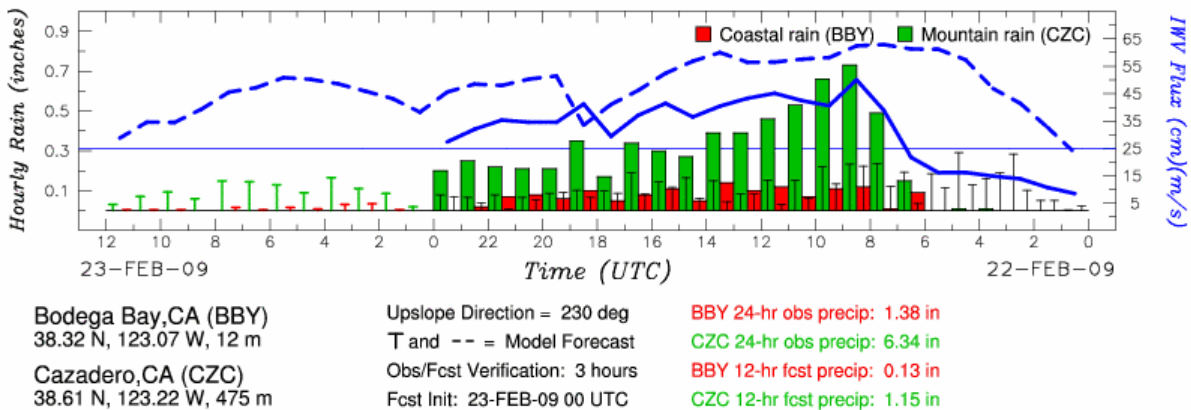

Figure 14. *Bottom panel of the coastal atmospheric river monitoring and early warning system Web display. The forecasted and observed bulk integrated water vapor flux are represented by the blue dashed and solid curves, respectively. The atmospheric river threshold for this flux (Neiman et al. 2009) is shown by the thin blue horizontal line. The observed precipitation at the coast (mountains) is represented by the red (green) solid bars. The forecasted precipitation during the observing period is represented by the black T posts. For the forecast-only period, the color of the T posts reverts to the coast/mountain distinction described above.*
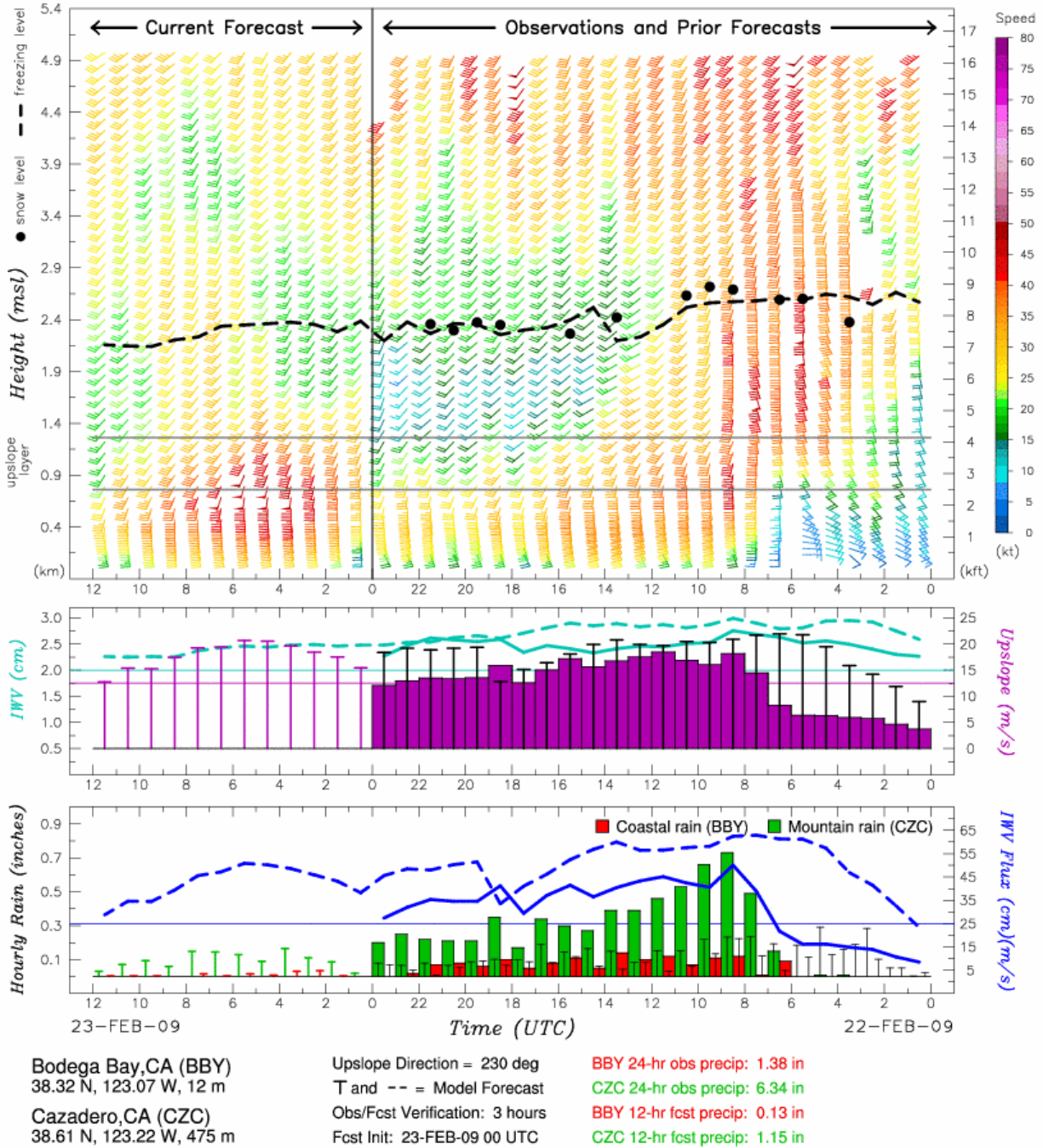
11

Figure 15. *The coastal atmospheric river monitoring and early warning system display as it was shown with hourly updates on the Web (http://www.etl.noaa.gov/et7/data/) during the wintertime beginning in February 2009.*
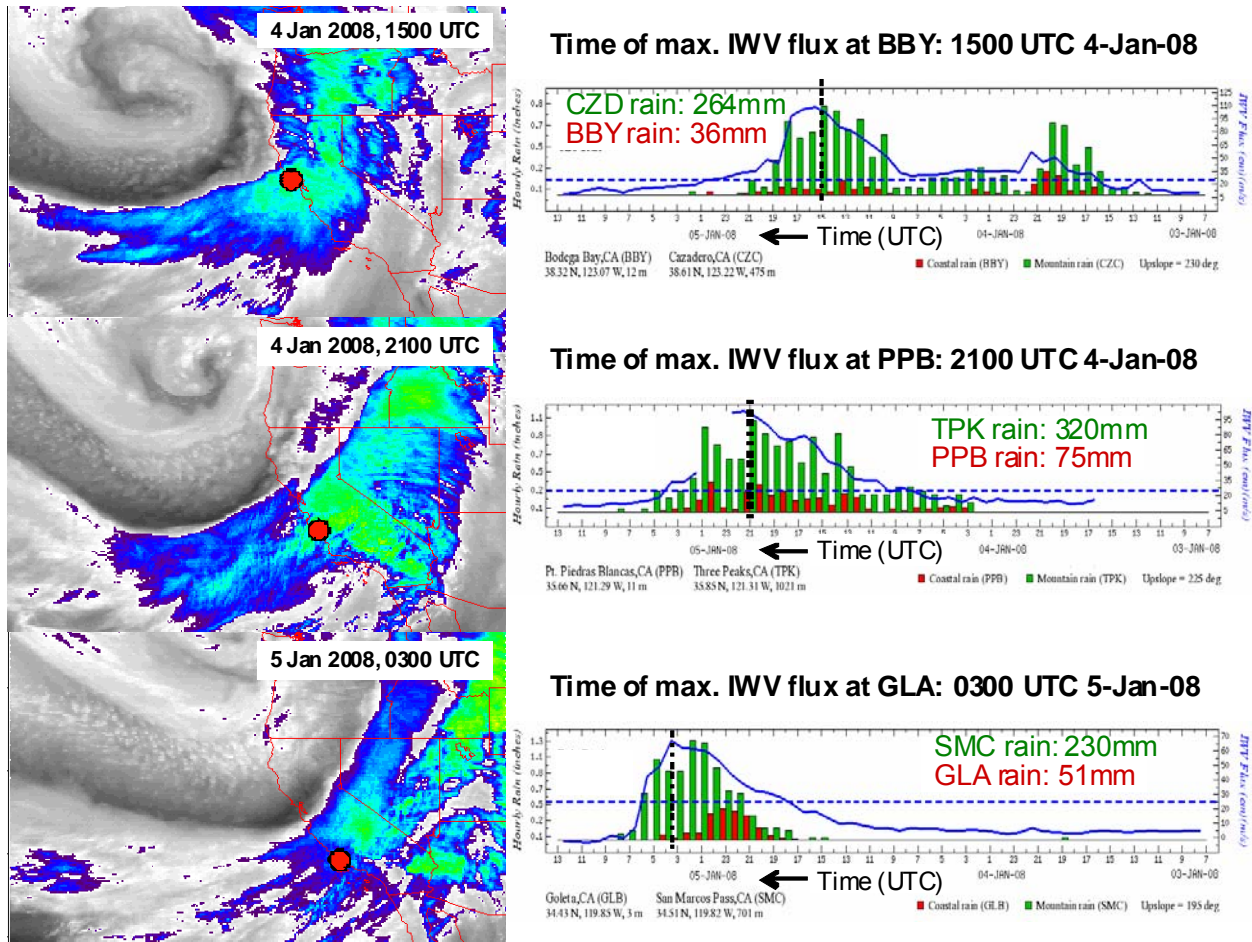
Figure 16. *Series of GOES IR satellite images for a powerful winter storm that impacted California in January 2008 (left). Image dates and times are indicated as are the locations (red dots) of three atmospheric river observatories (AROs) deployed along the coast. The corresponding displays (right) of bulk integrated water vapor flux (blue curves) and rainfall vertical bars as in Fig. 14, except without the numerical model output.*

6. ACKNOWLEDGMENTS

7. REFERENCES

Anagnostou, E. N., and C. Kummerow, 1997: Stratiform and convective classification of rainfall using SSM/I 85-GHz brightness temperature observations. *J. Atmos. Oceanic Technol.,* **14,** 570–575.

Battan, L. J., 1959: *Radar Meteorology.* University of Chicago Press, 161 pp.

Bevis, B. G., S. Bussinger, T. A. Herring, C. Rocken, R. A. Anthes, and R. H. Ware, 1992: GPS

13

Meteorology: Remote sensing of atmospheric water vapor using the Global Positioning System. *J. Geophys. Res.*, **97**, 15787–15801.

Carter, D. A., K. S. Gage, W. L. Ecklund, W. M. Angevine, P. E. Johnston, A. C. Riddle, J. S. Wilson, and C. R. Williams, 1995: Developments in UHF lower tropospheric wind profiling at NOAA's Aeronomy Laboratory. *Radio Sci.*, **30**, 997–1001.

Jankov, I., P. J. Schultz, C. J. Anderson, and S. E. Koch, 2007: The impact of different physical parameterizations and their interactions on cold season QPF in the American River Basin. *J. Hydrometeor.*, **8**, 1141–1151.

Leung, L. R., and Y. Qian, 2009: Atmospheric rivers induced heavy precipitation and flooding in the western U.S. simulated by the WRF regional climate model, *Geophys. Res. Lett.*, **36**, L03820, doi:10.1029/2008GL036445.

Martner, B.E., S.E. Yuter, A.B. White, S.Y. Matrosov, D.E. Kingsmill, and F.M. Ralph, 2007: Raindrop size distributions and rain characteristics in California coastal rainfall for periods with and without a radar brightband. *J. Hydrometeor.*, **9**, 408–425.

Neiman, P. J., F. M. Ralph, A. B. White, D. E. Kingsmill, and P. O. G. Persson, 2002: The statistical relationship between upslope flow and rainfall in California's Coastal Mountains: Observations during CALJET. *Mon. Wea. Rev.*, **130**, 1468–1492.

Neiman, P. J., F. M. Ralph, G. A. Wick, J. D. Lundquist, and M. D. Dettinger, 2008: Meteorological characteristics and overland precipitation impacts of atmospheric rivers affecting the West Coast of North America based on eight years of SSM/I satellite observations. *J. Hydrometeor.*, **9**, 22–47.

Neiman, P. J., A. B. White, F. M. Ralph, D. J. Gottas, and S. I. Gutman, 2009: A water vapour flux tool for precipitation forecasting. *Proc. Institution of Civil Engineers–Water Management*, **162**, 83–94.

Ralph, F. M., P. J. Neiman, and G. A. Wick, 2004: Satellite and CALJET aircraft observations of atmospheric rivers over the eastern North-Pacific Ocean during the winter of 1997/98. *Mon. Wea. Rev.*, **132**, 1721–1745.

Ralph, F. M., P. J. Neiman, and R. Rotunno, 2005: Dropsonde observations in low-level jets over the Northeastern Pacific Ocean from CALJET-1998 and PACJET-2001: Mean vertical-profile and atmospheric-river characteristics. *Mon. Wea. Rev.*, **133**, 889–910.

Ralph, F. M., P. J. Neiman, G. A. Wick, S. I. Gutman, M. D. Dettinger, C. R. Cayan, and A. B. White, 2006: Flooding on California's Russian River: The role of atmospheric rivers. *Geophys. Res. Lett.*, **33**, L13801, doi:10.1029/2006 GL026689.

White, A. B., J. R. Jordan, B. E. Martner, F. M. Ralph, and B. W. Bartram, 2000: Extending the dynamic range of an S-Band radar for cloud and precipitation studies, *J. Atmos. Oceanic Technol.*, **17**, 1226–1234.

White, A. B., D. J. Gottas, E. T. Strem, F. M. Ralph, and P. J. Neiman, 2002: An automated brightband height detection algorithm for use with Doppler radar spectral moments, *J. Atmos. Oceanic Technol.*, **19**, 687-697.

White, A. B., P. J. Neiman, F. M. Ralph, D. E. Kingsmill, and P. O. G. Persson, 2003: Coastal orographic rainfall processes observed by radar during the California Land-falling Jets Experiment. *J. Hydrometeor.*, **4**, 264–282.

White, A. B., F. M. Ralph, J. R. Jordan, C. W. King, D. J. Gottas, P. J. Neiman, L. Bianco, and D. E. White, 2007: Expanding the NOAA Profiler Network: Technology evaluation and new applications for the coastal environment. *Proc., 7th Conf. on Coastal Atmos. and Oceanic Prediction and Processes,* 10-13 Sep., 2007, San Diego, California, AMS Boston, 26 pp.

White, A. B., D. J. Gottas, A. F. Henkel, P. J. Neiman, F. M. Ralph, and S. I. Gutman, 2009: Developing a performance measure for snow-level forecasts. *J. Hydrometeor.*, submitted.

Zhu, Y., and R. E. Newell, 1998: A proposed algorithm for moisture fluxes from atmospheric rivers, *Mon. Weather Rev.*, **126**, 725–735.